

# Phase-space dynamics of Alfvén mode chirping

Cite as: Phys. Plasmas **27**, 052108 (2020); <https://doi.org/10.1063/5.0004610>

Submitted: 14 February 2020 . Accepted: 05 May 2020 . Published Online: 28 May 2020

R. B. White , V. N. Duarte , N. N. Gorelenkov , E. D. Fredrickson , and M. Podesta 



View Online



Export Citation




CrossMark



**NEW!**

Sign up for topic alerts  
New articles delivered to your inbox



# Phase-space dynamics of Alfvén mode chirping

Cite as: Phys. Plasmas **27**, 052108 (2020); doi: 10.1063/5.0004610

Submitted: 14 February 2020 · Accepted: 5 May 2020 ·

Published Online: 28 May 2020



View Online



Export Citation



CrossMark

R. B. White,<sup>a)</sup> V. N. Duarte, N. N. Gorelenkov, E. D. Fredrickson, and M. Podesta

## AFFILIATIONS

Princeton Plasma Physics Laboratory, Princeton University, Princeton, New Jersey 08543, USA

<sup>a)</sup> Author to whom correspondence should be addressed: [rwhite@pppl.gov](mailto:rwhite@pppl.gov)

## ABSTRACT

In tokamak discharges, toroidal Alfvén eigenmodes often experience complex semi-periodic frequency modulation known as chirping. These events modify the local high energy particle distribution and are expected to occur in many future fusion devices, which include energetic beams or fusion products. This paper presents a study of simulations of mode chirping made in order to better understand its phase-space properties in a realistic tokamak configuration. We find a mechanism that permits rapid repeated chirping with strong amplitude variation in each chirp. Each chirp is associated with an amplitude crash to low magnitude and local manipulation of the density gradients through a shift of mode phase through  $\pi$ . The chirping produces high density clumps, which propagate down the fast ion density gradient and low density holes that propagate up the density gradient away from the resonance. This flow of particles across the resonance provides an energy source and local gradients for repeated chirping.

Published under license by AIP Publishing. <https://doi.org/10.1063/5.0004610>

## I. INTRODUCTION

Chirping is a nonlinear resonance phenomenon that involves a complex frequency modulation of a single Alfvén mode, causing also local particle distribution modification, observed experimentally in many fusion devices<sup>1–10</sup> and in other plasmas containing an inverted high energy particle population.<sup>11</sup> Predictions indicate that the occurrence of Alfvén chirping cannot be ruled out in ITER.<sup>12</sup> Chirping happens on a millisecond timescale and can cause the convective ejection of fast ions in bursts, which can damage the vessel through a concentrated stream of highly energized impinging particles. It has been simulated using several codes.<sup>13–22</sup> It is a good test for analytical models and numerical simulation because of the complexity of the behavior.

An example of continuous multiple chirping on NSTX<sup>23</sup> in shot 113201 is shown in Fig. 1. There is a rapid chirping of the mode frequency, with the production of upward and downward excursions, sometimes almost up–down symmetric and sometimes very one sided.

The purpose of this paper is to employ a guiding-center code to elucidate the complex underlying dynamics of the phase-space structures sustaining the chirps in realistic tokamak geometry. This type of study has been carried out before in an idealized one-dimensional bump-on-tail setting.<sup>24</sup> Besides the motion of self-trapped holes and clumps, we find a rich evolution pattern in the resonance island structure of the original eigenmode. At each chirp, the mode amplitude is found to be subject to a massive crash in amplitude. By a phase shift of  $\pi$ , the mode is able to tap the free energy stored in the gradients in the

vicinity of where the hyperbolic points were previously located, i.e., at the edge of the former islands. The amplitude rebounds due to inverse Landau damping with the elliptic island structure having a phase shift of nearly  $\pi$  (with respect to the island structure before the amplitude crash), with the shift maximizing the energy extraction by the mode.

In Sec. II, we review the guiding center formalism and the means of advancing in time the Alfvén mode amplitude and phase, as well as the density modification produced by the mode. In Sec. III, we discuss the properties of the mode-particle resonance responsible for the chirping; in Sec. IV, we discuss details of the chirping; in Sec. V, we present clump-hole formation; and in Sec. VI, the conclusion.

## II. GUIDING CENTER FORMALISM

Chirping is common in discharges in which toroidal Alfvén eigenmodes (TAE) are excited. There is no need to select particular equilibria or particle distributions to study this phenomenon, provided the distribution has gradients to destabilize the TAE mode, damping is strong enough to make the mode marginal, and collisions are weak. We thus use a generic equilibrium and do not attempt to reproduce specific examples of chirping seen in a particular device. The equilibrium and  $q$  profile used in this study are shown in Fig. 2. The  $q$  profile, the local field line helicity, is a simple quadratic function of the minor radius. The on-axis magnetic field was  $B = 4.9$  kG.

The equilibrium magnetic field is given by

$$\vec{B} = g\nabla\zeta + I\nabla\theta + \delta\nabla\psi_p, \quad (1)$$

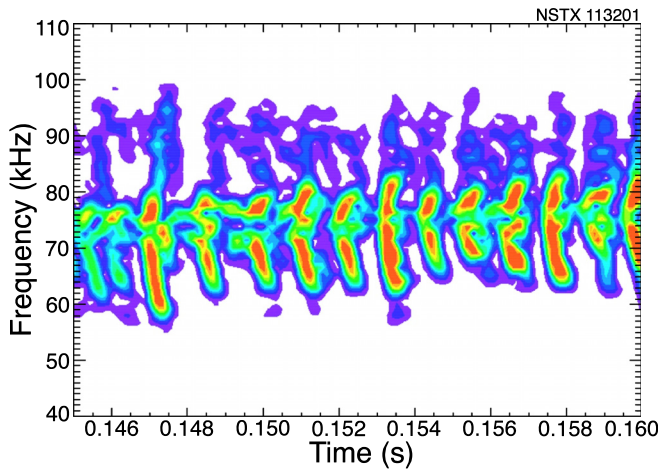


FIG. 1. Frequency spectrum of a sequence of chirps observed in NSTX in shot 113201 using Fourier integration.

where  $\theta$  and  $\zeta$  are poloidal and toroidal coordinates and  $\psi_p$  is the poloidal flux, and in an axisymmetric equilibrium using Boozer coordinates,  $g$  and  $I$  are functions of  $\psi_p$  only. The perturbation has the form  $\delta\vec{B} = \nabla \times \alpha\vec{B}$  and  $\alpha$  and an electric potential  $\Phi$  have the Fourier expansions

$$\alpha = \sum_{m,n} A_n \alpha_{m,n}(\psi_p) \sin(\Omega_{mn}), \quad \Phi = \sum_{m,n} A_n \Phi_{m,n}(\psi_p) \sin(\Omega_{mn}), \quad (2)$$

where  $n$  refers to a single mode with definite toroidal mode number  $n$  and frequency  $\omega_n$ , and the sum is over toroidal and poloidal harmonics  $m$  with  $\Omega_{mn} = n\zeta - m\theta - \omega_n t - \phi_n$ , with  $\phi_n$  giving the time dependent mode phase modification. For ideal modes, the electric

potential  $\Phi$  is chosen to cancel the parallel electric field induced by  $d\vec{B}/dt$ , requiring

$$\sum_{m,n} \omega_n B \alpha_{m,n} \cos(\Omega_{mn}) - \vec{B} \cdot \nabla \Phi / B = 0$$

to give in Boozer coordinates

$$(gq + I)\omega_n \alpha_{mn} = (nq - m)\Phi_{mn}.$$

The perturbation  $\alpha$  is related to the ideal displacement  $\vec{\xi}$ , through<sup>25</sup>

$$\alpha_{mn} = \frac{(m/q - n)}{(mg + nI)} \xi_{mn}^\psi.$$

The eigenfunctions produced with the code NOVA-K<sup>26</sup> are normalized with the largest harmonic  $\xi_{mn}^\psi(\psi_p)$  having maximum amplitude 1. Thus, the amplitude  $A_n$  is the magnitude of the ideal displacement caused by this harmonic, normalized to the major radius  $R$ .

The equations of motion in Hamiltonian form are<sup>25,27</sup>

$$\begin{aligned} \dot{\theta} &= \frac{\partial H}{\partial P_\theta} & \dot{P}_\theta &= -\frac{\partial H}{\partial \theta}, \\ \dot{\zeta} &= \frac{\partial H}{\partial P_\zeta} & \dot{P}_\zeta &= -\frac{\partial H}{\partial \zeta}, \end{aligned} \quad (3)$$

where canonical momenta are

$$P_\zeta = g\rho_\parallel - \psi_p, \quad P_\theta = \psi + \rho_\parallel I \quad (4)$$

and  $\psi$  is the toroidal flux, with  $d\psi/d\psi_p = q(\psi_p)$ , the field line helicity, and  $\rho_\parallel = v_\parallel/B$ , with  $v_\parallel = \vec{v} \cdot \vec{B}/B$ . The Hamiltonian is

$$H = \frac{(\rho_\parallel - \alpha)^2 B^2}{2} + \mu B + \Phi. \quad (5)$$

The modification of the particle distribution by the mode is carried out using a  $\delta f$  formalism. Write the particle distribution as

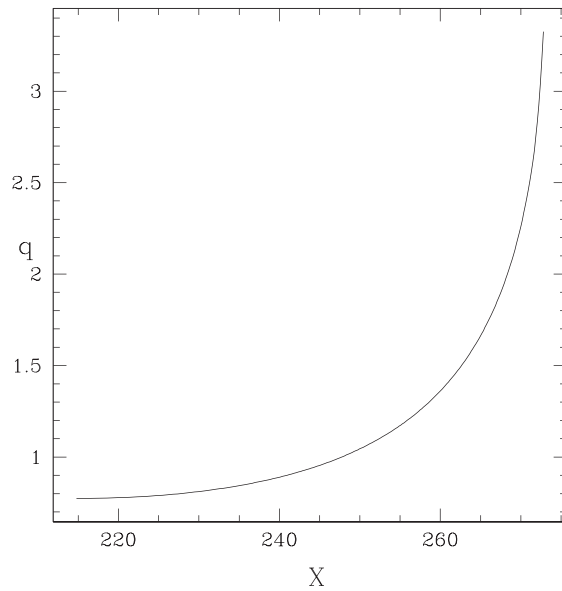
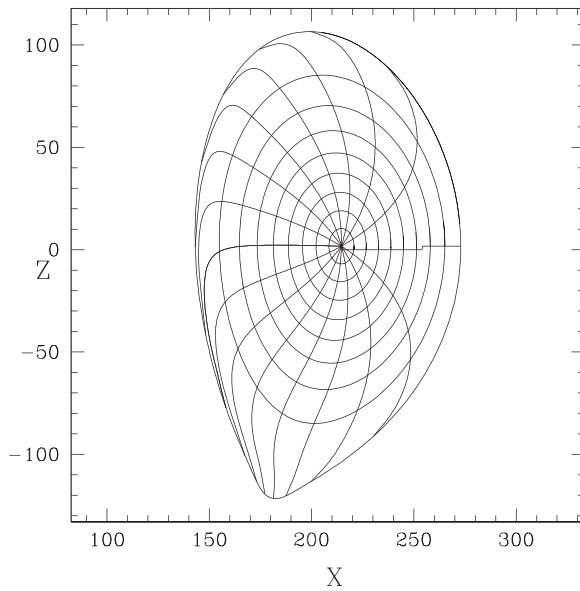


FIG. 2. Equilibrium and  $q$  profile used in the simulations.

$f = f_0 + \delta f$ , where the distribution in the absence of the modes  $f_0$  is a function of energy  $E$ , magnetic moment  $\mu$ , and  $P_\zeta$  and is independent of time. Following particle orbits  $df/dt = 0$ , and to order  $\alpha$ ,

$$\frac{d}{dt} \delta f = -\partial_E f_0 \dot{E} - \partial_P f_0 \dot{P}_\zeta, \quad (6)$$

where we neglect changes in  $\mu$  since we are considering a collisionless guiding center simulation. The numerically loaded and evolved distribution function is  $g(\psi_p, \theta, \zeta, \rho_{||}, t)$  with  $dg/dt = 0$ . The distribution  $g$  has the Klimontovich representation

$$g(\psi_p, \theta, \zeta, \rho_{||}, t) = \sum_j \delta(\psi_p - \psi_{p,j}(t)) \delta(\theta - \theta_j(t)) \times \delta(\zeta - \zeta_j(t)) \delta(\rho_{||} - \rho_{||,j}(t)), \quad (7)$$

with  $j$  the particle index and  $\delta f$  represented by

$$\delta f(\psi_p, \theta, \zeta, \rho_{||}, t) = \sum_j w_j \delta(\psi_p - \psi_{p,j}(t)) \delta(\theta - \theta_j(t)) \times \delta(\zeta - \zeta_j(t)) \delta(\rho_{||} - \rho_{||,j}(t)). \quad (8)$$

The particle weight  $w = \delta f/g$  and we find from Eq. (6),

$$\begin{aligned} dw/dt &= -(1/g) df_0/dt = -(f_0/g) d \ln(f_0)/dt \\ &= -(f/g - w) d \ln(f_0)/dt \end{aligned} \quad (9)$$

and  $f/g$  is constant in time and given by the value at  $t=0$ . Normally, simulations assume that the initial perturbation of the distribution  $\delta f$  is zero, so initially,  $w(0) = 0$  for all particles.

Stepping equations for the mode amplitude and phase were previously derived,<sup>28,29</sup>

$$\frac{dA_n}{dt} = \frac{-\nu_A^2}{D_n \omega_n} \sum_{j,m} w_{n,j} \left[ \rho_{||} B^2 \alpha_{mn}(\psi_p) - \Phi_{mn}(\psi_p) \right] \cos(\Omega_{mn}) - \gamma_d A_n, \quad (10)$$

$$\frac{d\phi_n}{dt} = \frac{-\nu_A^2}{D_n \omega_n A_n} \sum_{j,m} w_{n,j} \left[ \rho_{||} B^2 \alpha_{mn}(\psi_p) - \Phi_{mn}(\psi_p) \right] \sin(\Omega_{mn}), \quad (11)$$

with  $\nu_A$  the Alfvén frequency,  $D_n = 4\pi^2 \sum_m \int \zeta_{mn}^2(\psi_p) d\psi_p$ ,  $j$  the particle index and  $\psi_p, \theta, \zeta$  the position, and  $\rho_{||}$  the normalized parallel velocity of particle  $j$ . Original derivations of these equations assumed that the individual modes were orthogonal and normalized to one. This is not the case with multiple poloidal harmonics, and  $D_n$  is required. The modes are resonant with and destabilized by a high energy injected beam or fusion alpha particles, so the particles refer to high energy ions. The linear damping rate  $\gamma_d$  is due to the continuum, trapped particle collisional damping, electron and thermal ion Landau damping, and radiation, all terms in the sums are evaluated at the coordinates of particle  $j$ , and  $w_{n,j}$  is the  $\delta f$  weight of particle  $j$  for mode  $n$ . The damping is calculated by NOVA-K for simulating experimentally observed chirps, but is a free input parameter for generic cases not related to an experiment.

### III. RESONANCE

For a single mode, the change in energy  $E$  and  $P_\zeta$  due to the mode are related, since if  $H = H(n\zeta - m\theta - \omega t)$ ,

$$\partial_\zeta H = -n \partial_t H / \omega, \quad n dE = \omega dP_\zeta. \quad (12)$$

Unperturbed orbits have toroidal and poloidal periodicities  $\omega_\zeta$ , and  $\omega_\theta$ , and the generalized resonance condition is that the mode phase due to mode frequency  $\omega$  returns to the same value when a particle also repeats periodic motion,

$$l\omega = p\omega_\theta + n\omega_\zeta, \quad (13)$$

where  $l, m, p$ , and  $n$  are integers. Note that this  $p$  value is not the poloidal mode number  $m$  of a perturbation— $p$  is determined by orbital dynamics, but for resonance with the mode, it is typically near a poloidal harmonic  $m$  of the mode. For a TAE mode to be destabilized, this frequency must match the frequency of a gap toroidal Alfvén mode<sup>30</sup>

$$\omega = \frac{V_A(r_0)}{2Rq(r_0)}, \quad (14)$$

where the mode exists in the gap between modes with  $q = m/n$  and  $q = (m+1)/n$  and  $r = r_0$  with  $q(r_0) = (m+1/2)/n$ , and  $V_A = B/\sqrt{4\pi n_i m_i}$  is the local Alfvén velocity. For mode excitation, the drive due to the local density gradient must be greater than the damping, but for chirping to occur, the damping must also be large so the mode is near marginal stability.

To find the form of the resonance, we examine a Poincaré section produced by this Hamiltonian. Set  $n\zeta - \omega t = 2\pi k$  with  $k$  integer to produce the Poincaré points and introduce a simple perturbation,  $H_I = -V \cos(n\zeta - m\theta - \omega t - \phi)$ . Since the Hamiltonian is quadratic in the canonical momentum  $P_\zeta$ , expand it around the value of  $P_\zeta$  for which the resonance holds,  $P_0$ . We then have

$$H \simeq c \frac{(P_\zeta - P_0)^2}{2} - V \cos(m\theta + \phi), \quad (15)$$

with  $c$  a constant depending on local equilibrium parameters.

In Fig. 3 are shown the resulting Poincaré surfaces of particle trajectories in the plane of  $P_\zeta$  and  $Q = p\theta + \phi$ , where we take  $P_0 = 0$

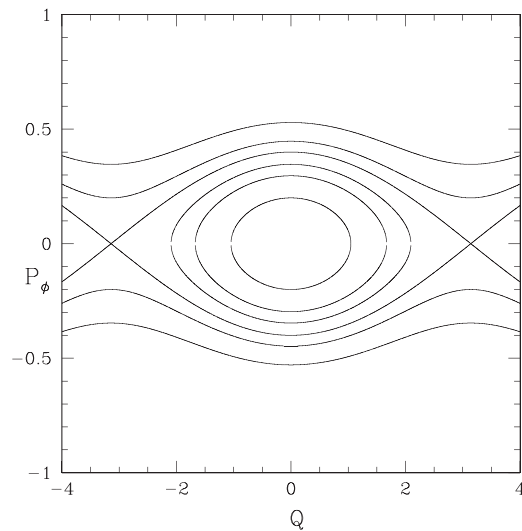


FIG. 3. Poincaré surfaces of a resonance in a tokamak produced by a mode depending on  $n\zeta - m\theta - \omega t$  with  $Q = p\theta + \phi$ , where  $p$  is an integer and  $\phi$  is a phase.

for simplicity. Note that the Hamiltonian is time dependent, so  $E$  is not conserved, and in fact through Eq. (12) the trajectories in the energy variable have the same form as these in  $P_\zeta$ . Thus,  $H$  in Eq. (15) is no longer the Hamiltonian, which is time dependent, setting  $H = \text{const}$  only defines the trajectories in the Poincaré section. Expanding near  $Q = 0$ , we have  $H \simeq cP_\zeta^2/2 - V(1 - Q^2/2)$  and we find this to be an elliptic point (the origin is  $H = -V$ ). Expanding about  $Q = \pi$  with  $dQ = Q - \pi$ , we find  $H \simeq cP_\zeta^2/2 + V(1 - dQ^2)$ , a hyperbolic point (the X point) and thus, the separatrix is given by the lines  $H = V$ . The width of the resonance is

$$\delta P_\zeta = 4\sqrt{V/c}. \tag{16}$$

All particles within the separatrix are trapped in the resonance and circulate around the elliptic point. As they do this, both the energy and the canonical momentum  $P_\zeta$  change periodically. Particles outside the separatrix are not trapped, but they still experience change of  $P_\zeta$  and  $E$ , which is periodic and adiabatic. These particles stream to the right for  $P_\zeta > 0$  and to the left for  $P_\zeta < 0$ . All particles trapped in the resonance have mean motion  $d\zeta/d\theta = n/p$ .

To find the rate of rotation about the O-point and the streaming velocity, use the fact that  $H = \text{constant}$  defines the Poincaré surfaces, so use  $dH/dt = 0$ , giving

$$c(P_\zeta - P_0)\dot{P}_\zeta = V \sin(Q)\dot{Q}. \tag{17}$$

However,  $\dot{P}_\zeta = -\partial_\zeta H = nV\sin(Q)$ , giving for a particle trapped within the resonance

$$\dot{Q} \simeq n\sqrt{V/c}\sqrt{\cos(Q) - \cos(Q_0)}, \tag{18}$$

with  $Q_0$  the initial point of the trajectory. The time to complete an orbit around the elliptic point is  $T = 4 \int_0^{Q_0} dQ/\dot{Q}$ , giving

$$T = \frac{4}{n\sqrt{V}} \int_0^{Q_0} \frac{dQ}{\sqrt{\cos(Q) - \cos(Q_0)}}. \tag{19}$$

For small  $Q_0$ , this is  $T = 4/(n\sqrt{2V})$ , and for  $Q_0 = \pi$ , the integral diverges. The frequency about the elliptic point is proportional to the island width, or the square root of the perturbation amplitude, and it goes to zero as the separatrix is approached.

The dependence of the rotation rate on the distance from the elliptic point means that if there exists an initial density gradient complex mixing of the density occurs in the resonance interior, with the mixing bringing domains of very different density in close proximity and producing locally very strong gradients. Consider a point at the high density side of the elliptic point at distance  $r$  from it and another point on the low density side at distance  $r + \delta$  from it. At these points, the densities are very different, but in a few bounce times they will be adjacent. Density gradients within the resonance approach infinity everywhere. This leads to an irreversible flattening of the distribution and an increase in entropy within the resonance within a few periods, even with a low collision rate.

For a particle outside the separatrix, we have

$$\dot{Q} = nc(P_\zeta - P_0) = \pm n\sqrt{2c}\sqrt{H + V \cos(Q)}. \tag{20}$$

The streaming velocity is zero at the separatrix,  $H = V$ , and increases away from it, positive for  $P > P_0$  and negative for  $P < P_0$ . Also, outside the resonance, the sheared rotation moves neighboring domains

past one another, but they differ only infinitesimally in density, so no mixing is produced.

Additional small perturbations due to the presence of other modes produce a narrow chaotic domain about the separatrix and the hyperbolic point. Even if the resonance is large, this small broadening of the separatrix is not easily visible in a Poincaré section. It becomes readily apparent when multiple resonances approach overlap.

#### IV. CHIRP SIMULATION

To carry out chirp simulations, the fast ion particle distribution is constructed using a single value of the magnetic moment  $\mu$ , since it is conserved in collisionless guiding center simulations, with a density gradient, and with particles deposited along the line  $nE - \omega P_\zeta = \text{const}$ , with the constant and the range of variables chosen to ensure that the distribution covers the resonance. A small random spread of particles around this line is allowed, since with mode frequency modulation particles not exactly on the line are involved in mode resonance. The density of the initial distribution  $f_0$  is large at small minor radius (large  $P_\zeta$ ) and zero at the plasma edge (small  $P_\zeta$ ) so the initial gradient is  $df_0/dP_\zeta > 0$ . We choose a deuterium co-passing particle distribution with energy between 80 and 100 keV with  $\mu B = 2$  keV, and in the following, density refers always to the high energy particle density, the thermal plasma population only establishing the background equilibrium.

The perturbation used was an ideal mode with poloidal and toroidal mode numbers  $m/n = 6/5$  and the resulting resonance has four poloidal elliptic points. Following an orbit at the resonance location  $P_\zeta = 0.76$ , we find  $\dot{\theta} \simeq 1.08 \times 10^6$  and  $\dot{\zeta} \simeq 9.9 \times 10^5/s$ . The mode has a frequency of 100 kHz giving  $\omega = 6.28 \times 10^5/s$ , so we find  $\omega = p\dot{\theta} + n\dot{\zeta}$  with  $p = -4, n = 5$ .

The resonance is found using a kinetic Poincaré plot, plotting points only when a particle reaches a point with  $n\zeta - \omega t = 2k\pi$  with  $k$  integer. The resonance is shown in Fig. 4 for  $A = 10^{-4}$  (the amplitude normalization is with respect to the major radius). Also shown is the modification of the fast ion density  $\delta f$  produced, where here the variation  $\delta f$  is given by the time evolution of the particle weights, and this distribution is constructed with respect to the variable  $P_\zeta$ , a constant of the motion in the absence of the mode. The mode amplitude and phase are held constant and the simulation advanced for 100 toroidal transits, to allow the weights to adjust to the perturbation. The toroidal transit time of a characteristic particle in the distribution is a convenient unit of time; in this case, the particle energy was 85 keV and the transit time 4.7  $\mu s$ . We will refer to the resulting modification of the fast ion density profile with the terms cavity and peak, to distinguish them from the clumps and holes produced outside the resonance by the chirping process. The change in fast ion density results in a net motion of particles downward in  $P_\zeta$ , toward the plasma edge.

To study the time evolution of a chirp, we examine the amplitude, growth rate, and mode phase as a function of time, and also find detailed time evolution of the frequency spectrum and  $\delta f$ . A chirp occurs when an Alfvén mode encounters low collisions and strong damping. Initially, the mode grows, but with weak collisions unable to reestablish the fast ion density gradient within the resonance, the mode flattens the profile and the drive drops to zero. The damping then ensures a collapse to a small amplitude (see, for example, Fig. 6).

Analysis of the mode frequency spectrum is done using the Wigner distribution of quasi-probability<sup>22,31,32</sup>

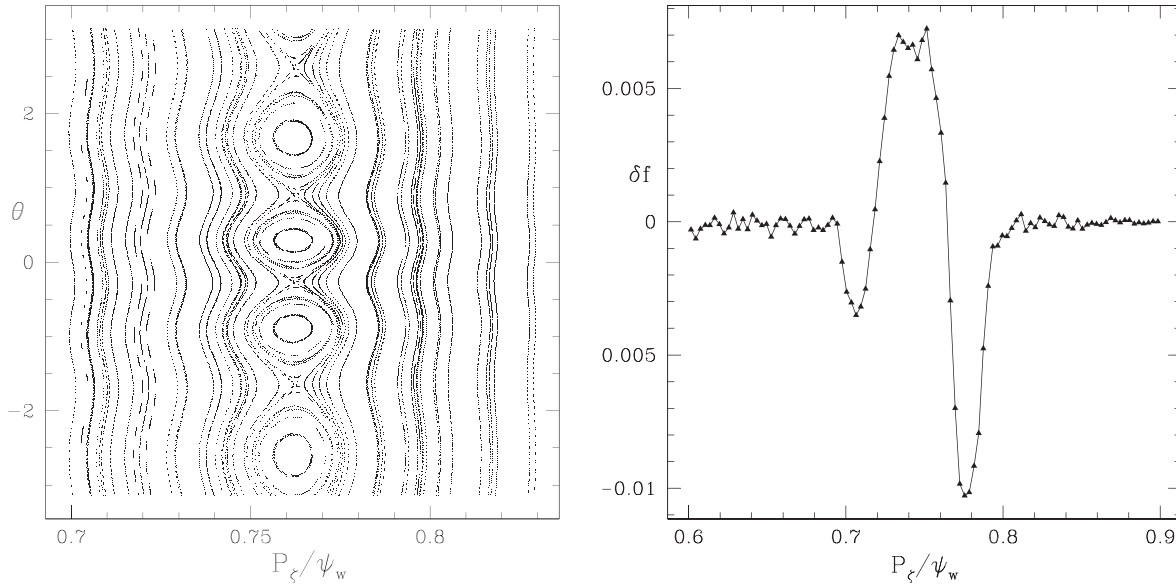


FIG. 4. Resonance,  $A = 10^{-4}$ , and  $\delta f$  produced, scale arbitrary.

$$W(t, \omega_k) = \int_{-T}^T \Phi^*(t+q)\Phi(t-q)e^{-2i\omega_k q} dq, \quad (21)$$

where we consider a single mode with frequency  $\omega$  and  $\Phi(t) = A(t) [\cos(\omega t + \phi(t)) + i \sin(\omega t + \phi(t))]$ . The spectrum given by  $\omega_k$  is chosen to span the mode frequency with a range large enough to include the frequency modulation due to the chirps. We used 51 values of  $\omega_k$ . The frequency modulation consists primarily of the development of sidebands, which depart from the main frequency. This nonlinear analysis provides a more detailed picture of the spectrum than a simple Fourier decomposition.

The frequency modulation of one of the chirps studied in detail is shown in Fig. 5. To obtain a good representation of this process using the Wigner integral, one must experiment with the range of the spectrum examined as well as the integration time. The integration range used was nine toroidal transits and the frequency spectrum included 20 percent variation both above and below the mode frequency.

In Fig. 6 are shown the amplitude and the growth rate as a function of time. Four chirps are present, the strongest being the second and third, with amplitude minima at about  $t = 55$  and  $t = 65$  transits. The damping is seen to be equal to more than half of the value of the initial growth rate.

In Fig. 7 are shown the frequency modulation and the mode phase as a function of time, produced by the particle distribution through Eqs. (10) and (11). The frequency modulation consists of delta function frequency bursts, giving a phase change of approximately  $\pi$  at each amplitude crash when the amplitude reaches a small value and the chirp occurs. Small fluctuations of density in the vicinity of the hyperbolic points modify the shift to differ somewhat from  $\pi$ . The amplitude does not reach zero, and in fact, the speed with which the phase change occurs depends on the magnitude of the amplitude, the change of  $\pi$  occurring more rapidly when the amplitude is smaller.

The changes at  $t = 40$  and  $t = 73$ , where the minimum amplitude is larger, are much slower than those at  $t = 55$  and  $t = 65$ , corresponding to the  $1/A$  factor in Eq. (11).

The sign of the phase changes at successive chirps appears to be random, probably produced by small density fluctuations near the island hyperbolic points. The phase shift places the elliptic point of the resonance at the previous location of a hyperbolic point, where the particle gradient is a maximum, and strong growth resumes. The growth following the collapse is stronger than the initial mode growth, indicating that at the moment of amplitude crash the density gradient at the initial hyperbolic point is even steeper than the original gradient.

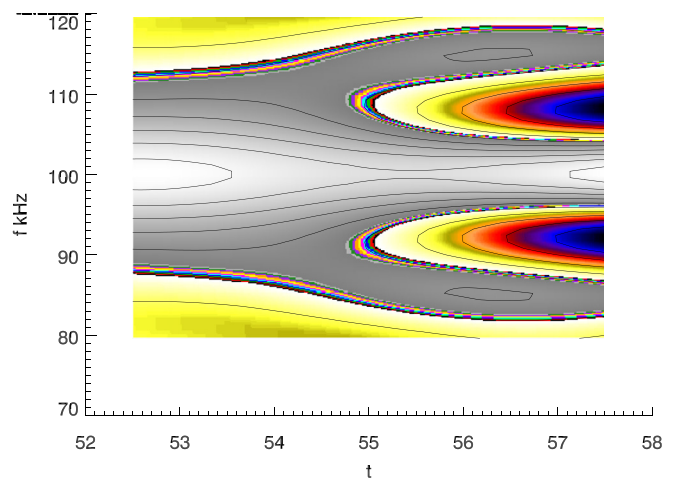
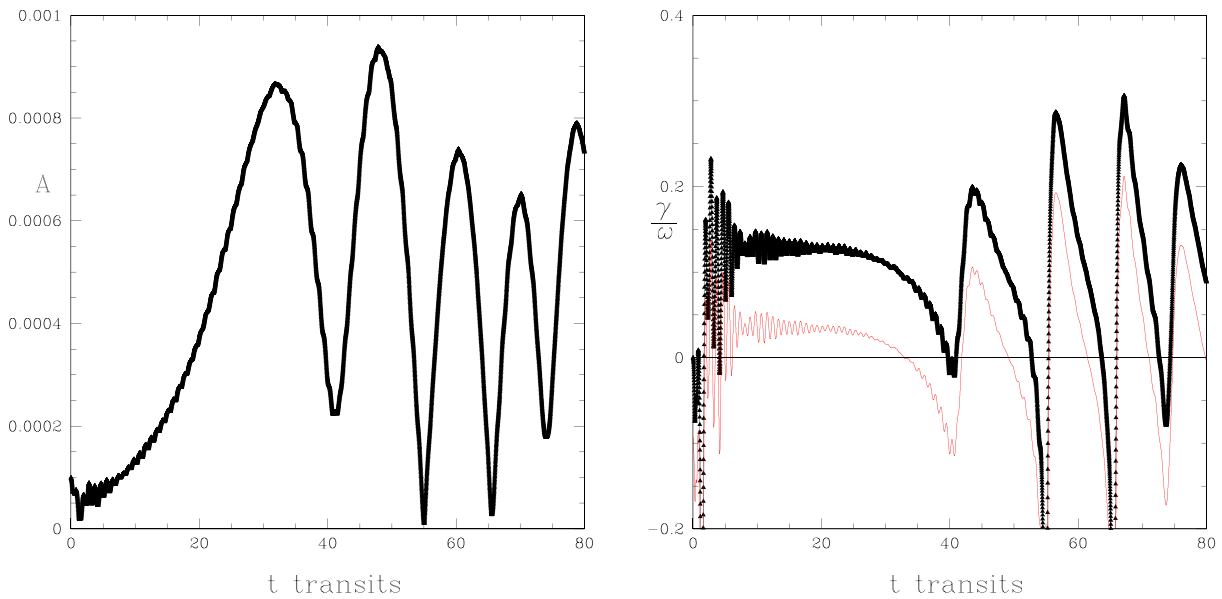


FIG. 5. Frequency modulation during a chirp, showing the production of two sidebands with frequency changes of about 15%.



**FIG. 6.** Time evolution of the amplitude  $A$  and the growth rate  $\gamma$ . The mode amplitude experiences periodic crashes at each chirp. In the plot of  $\gamma$ , the red line shows the net growth including the mode damping and the black line represents  $\gamma$  in the absence of damping. The growth rate after each crash is larger than the initial linear growth rate.

A small constant in time phase change has been subtracted in this plot in order to clearly show the changes by  $\pi$ .

The development of the two sideband frequencies shown in Fig. 5 occurs at the moment of amplitude minimum and phase shift,  $t = 55$ . We note that phase shift has been observed in experimental data<sup>33,34</sup> as well as in simulations.<sup>35</sup>

We find it remarkable that the presence of a strong gradient near the previous hyperbolic point can through Eq. (11) produce a rapid

shift of the mode to take advantage of this energy source. This cycle can repeat indefinitely in simulations, and experiments often show continuous chirping during the whole time history of the Alfvén mode.

**V. CLUMP-HOLE FORMATION**

To see the modification of the density profile, we follow the time evolution of the density perturbation,  $\delta f$ . This is done using the weight  $w$ , by binning particles in two dimensions using  $P_\zeta$  and  $\theta$  at Poincaré

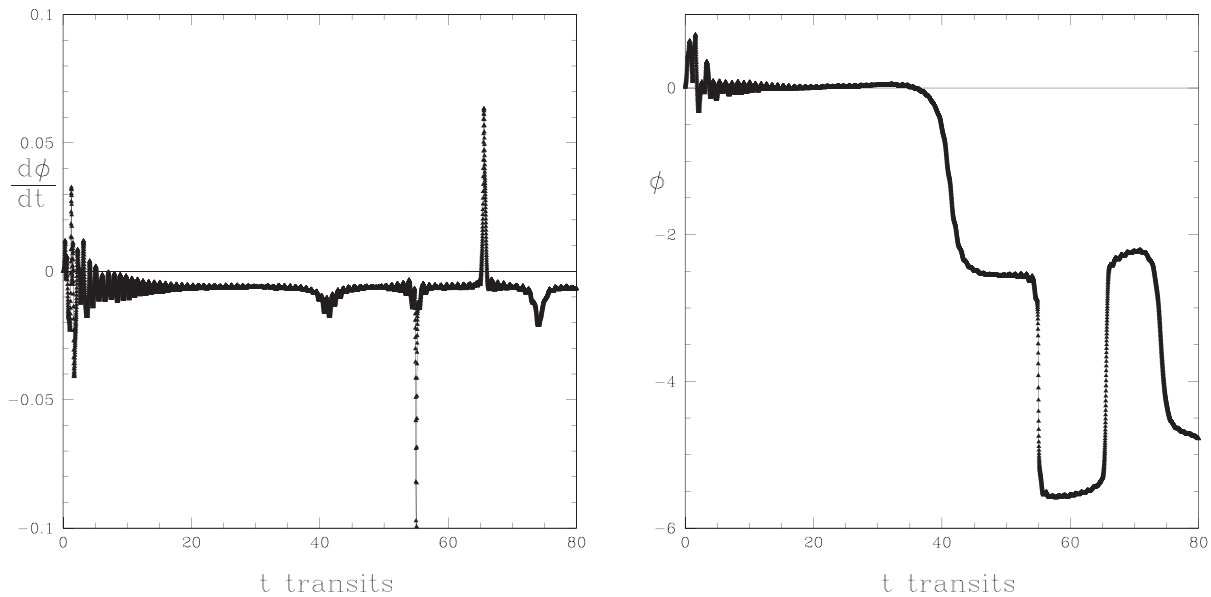


**FIG. 7.** Time evolution of frequency and phase, in units of toroidal transit times. A small frequency drift linear in time has been subtracted to show clearly the shift of approximately  $\pi$  at the amplitude minima.

times, insuring that particles have a fixed phase with respect to the mode,  $n\zeta - \omega t = 2\pi k$  with  $k$  integer. One million particles were used and data were collected at each toroidal transit, using 50 bins in each variable. In the simulation shown, the first chirps occur at  $t = 25, 36, 54, 68, 77,$  and  $85$  toroidal transits.

Examples of the evolution of  $\delta f$  are shown in Figs. 8 and 9. The simulation is for a time of 0.3 ms and includes several chirp events, similar to what is shown in Fig. 1. The initial magnitude of  $\delta f/f$  is  $10^{-7}$  and indicates small density depletion near the elliptic points and increase near the hyperbolic points, approximately equal in magnitude. For the full time history of the magnitudes, see Fig. 10. Rotational motion about the elliptic points transfers the density maxima downward and the minima upward. As the upper low density centers move to the right, they attach to additional small holes and pull them upward. The maximum absolute magnitude of  $\delta f/f$  in the holes and in the clumps is approximately equal and approaches  $4 \times 10^{-4}$ .

After the initial formation, the clumps drift leftward and the holes to the right, indicating that they are not attached to the resonance elliptic and hyperbolic points. This motion is more rapid at the times when the amplitude is a minimum, when the resonance width is small and a chirp is produced. The drift motion agrees with Eq. (20). After some toroidal transit times, the holes begin to drift upward and the clumps downward away from the resonance. The maximum separatrix width of the resonance is about  $\delta P_\zeta/\psi_w = 0.02$ , with  $\psi_w$  the

poloidal flux at the last closed flux surface, so the holes and clumps are self-organized density variations, drifting far from the resonance.

In Fig. 10 is shown the time history of the magnitude of the density perturbation as well as a history of the mean values of  $P_\zeta$  in clumps ( $\delta f > 0$ ) and holes ( $\delta f < 0$ ) showing steady motion of clumps down the density gradient and the holes up the gradient. The plot was obtained by finding the mean values of  $P_\zeta$ ,  $\int P_\zeta \delta f dP_\zeta d\theta / \int \delta f dP_\zeta d\theta$  with the integrals restricted to domains with  $\delta f$  positive for clumps and negative for holes. The holes, moving into a region of high density, are quickly dissipated by the sheared flow and cannot be followed very far. The clumps, moving into low density, are very stable and move toward the plasma edge.

In Fig. 11 is shown the time evolution of  $\delta f$  around the maximum mode amplitude occurring before a chirp. The shape and magnitude of the cavity around  $P_\zeta = 0.8$  and the peak at  $P_\zeta = 0.75$  change little in this period, the cavity broadening a little. There is a rapid sequence of density fluctuations at the edges of the cavity and the peak present at the time the mode reaches its maximum value, showing that small scale density fluctuations, in addition to the large clumps and holes, also give particle transport outward. This plot is made by binning particles using  $\delta f$  every time step and accumulating the data for  $1/10^{\text{th}}$  of a toroidal transit time to improve statistics. A total of  $10^6$  particles were used and there are 100 bins in canonical momentum  $P_\zeta$ . There are also 100 time steps per toroidal transit, so there are  $10^5$  particles per bin.

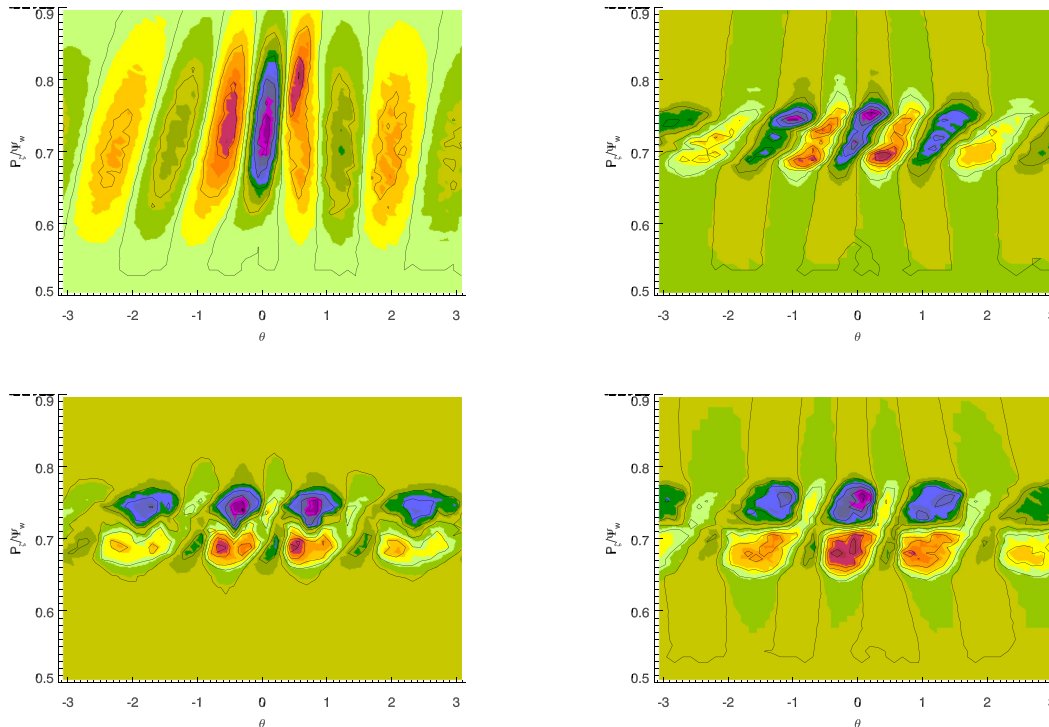


**FIG. 8.** Plots of  $\delta f$  at  $t = 1, t = 24, t = 53,$  and  $t = 84$ . Initially,  $\delta f$  is  $10^{-7}$ , and indicates small fast ion density depletion near the four elliptic points and increase near the hyperbolic points, extending vertically beyond the resonance. The maximum island width is only  $\delta P_\zeta = 0.02$ . The color bar shows both positive and negative  $\delta f$ , with the maximum absolute magnitudes approximately equal. The plots at  $t = 24, t = 53,$  and  $t = 84$  occur just before chirps, and high density streamers extending vertically from the clumps are visible. These occur at each chirp and are density peaks moving down to join the clumps.



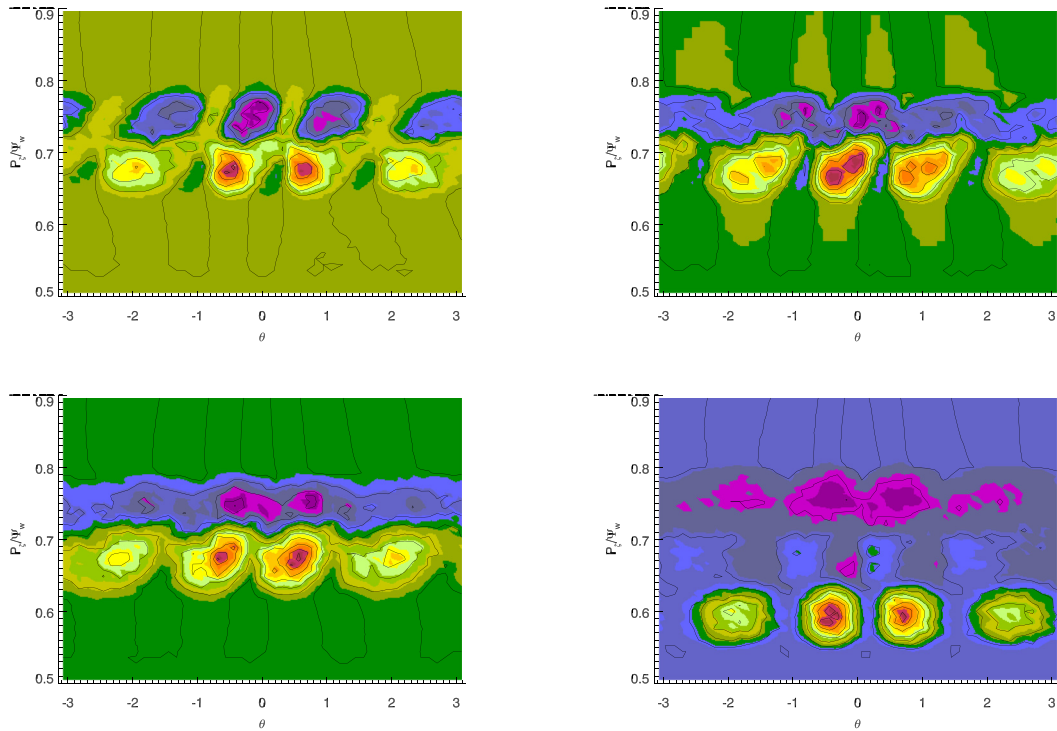


**FIG. 9.** Plots of  $\delta f$  at  $t = 100$ ,  $t = 120$ ,  $t = 200$ , and  $t = 500$ . The holes propagate upward away from the resonance and are torn apart from the sheared flow, and the clumps propagate downward, toward the plasma edge.

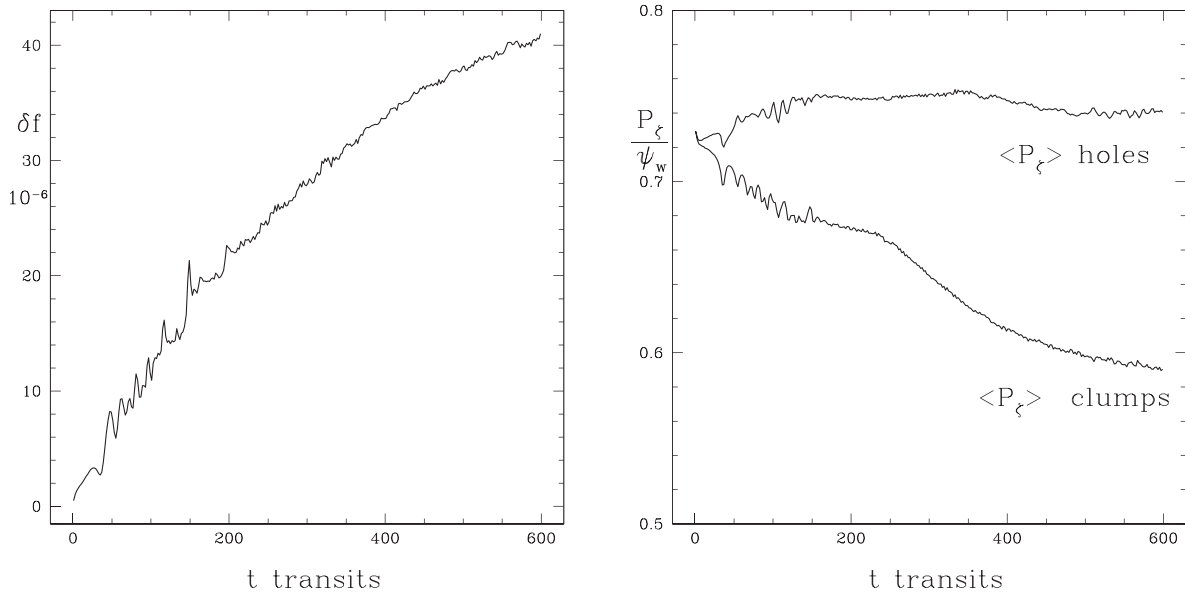


**FIG. 10.** Time evolution of the root mean square magnitude of  $\delta f$ , with the clumps and holes approximately equal in magnitude. Also shown is a history of the mean values of  $P_z$  in clumps ( $\delta f > 0$ ) and holes ( $\delta f < 0$ ) showing steady motion of the clumps down the density gradient. The holes move some distance up the gradient but are then destroyed by the velocity shear and cannot be followed very far.

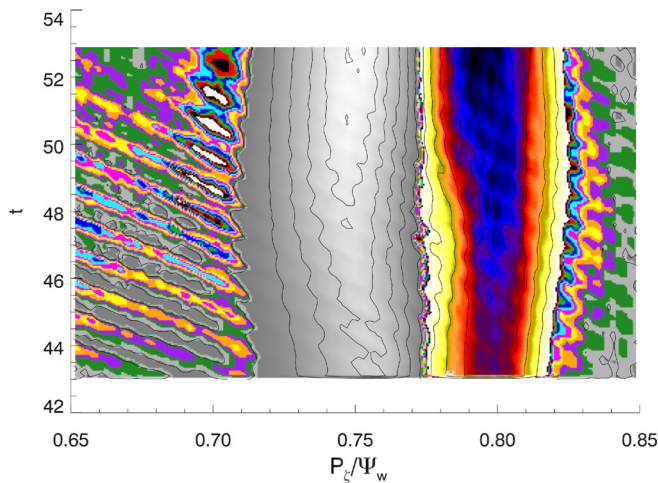


**FIG. 11.** Time evolution of  $\delta f$  showing a rapid sequence of small clumps and holes occurring around the amplitude maximum occurring before the amplitude crash at  $t = 54$ .

The steady production of clumps moving outward radially and holes moving inward produces a flow of particles across the resonance and serves to provide the energy for the continuous periodic chirping.

## VI. CONCLUSION

TAE mode chirping occurs when modes are near marginal stability with weak collisions. The mode initially grows until it has flattened the local density gradient sufficiently to eliminate the drive for growth. Large damping causes the approach to amplitude maximum to be very slow, and the continual strong resonance mixing causes excessive density flattening. The damping then causes a crash of the mode amplitude and a frequency chirp. At the amplitude minimum, there is a rapid shift of the mode phase through  $\pi$ , occurring in a time of one or two toroidal transits. When the mode has collapsed, the concentrations of particles surrounding the resonance form clumps and holes.<sup>14</sup> The shift of mode phase at the amplitude minimum places the elliptic point at a strong density gradient and the resulting growth leading to the next chirp is stronger than the initial linear growth rate of the mode. The large scale clumps and holes produced by the rotational transformation of initial weak density depressions and accumulations occurring near the elliptic and hyperbolic points of the resonance increase in magnitude, with the clumps moving outward and the holes moving inward. A non-chirping TAE mode typically saturates in amplitude, with particle collisions continually replenishing the density gradient within the resonance, and the resonance mixing providing the energy to balance the damping. The clump simulations are collisionless, and the damping is large. The continuous production of clumps and holes produces a net flow of particles down the density gradient across the resonance and supplies energy to drive the chirping.

## ACKNOWLEDGMENTS

Discussions with Andreas Bierwage are greatly appreciated. This work was supported by the U.S. Department of Energy (DOE) under Contract No. DE-AC02-09CH11466.

## DATA AVAILABILITY

The data that support the findings of this study are available from the corresponding author upon reasonable request. In particular, a film of the clump-hole formation is available.

## REFERENCES

- <sup>1</sup>E. D. Fredrickson, R. Bell, D. Darrow, G. Fu, N. Gorelenkov, B. LeBlanc, S. Medley, J. Menard, H. Park, L. Roquemore, S. A. Sabbagh, D. Stutman, K. Tritz, N. Crocker, S. Kubota, W. Peebles, K. C. Lee, and F. Levinton, *Phys. Plasmas* **13**, 056109 (2006).
- <sup>2</sup>W. W. Heidbrink, *Plasma Phys. Controlled Fusion* **37**, 937 (1995).
- <sup>3</sup>M. Podestà, R. Bell, A. Bortolon, N. Crocker, D. Darrow, A. Diallo, E. Fredrickson, G.-Y. Fu, N. Gorelenkov, W. Heidbrink, G. Kramer, S. Kubota, B. LeBlanc, S. Medley, and H. Yuh, *Nucl. Fusion* **52**, 094001 (2012).
- <sup>4</sup>C. Boswell, H. Berk, D. Borba, T. Johnson, S. Pinches, and S. Sharapov, *Phys. Lett. A* **358**, 154 (2006).
- <sup>5</sup>Y. Kusama, G. Kramer, H. Kimura, M. Saigusa, T. Ozeki, K. Tobita, T. Oikawa, K. Shinohara, T. Kondoh, M. Moriyama, F. Tchernychev, M. Nemoto, A. Morioka, M. Iwase, N. Isei, T. Fujita, S. Takeji, M. Kuriyama, R. Nazikian, G. Fu, K. Hill, and C. Cheng, *Nucl. Fusion* **39**, 1837 (1999).
- <sup>6</sup>M. P. Gryaznevich and S. E. Sharapov, *Plasma Phys. Controlled Fusion* **46**, S15 (2004).
- <sup>7</sup>L. Horvath, G. Papp, P. Lauber, G. Por, A. Gude, V. Igochine, B. Geiger, M. Maraschek, L. Guimaraes, V. Nikolaeva, G. Pokol, and ASDEX Upgrade Team, *Nucl. Fusion* **56**, 112003 (2016).
- <sup>8</sup>A. Melnikov, L. Eliseev, F. Castejon, C. Hidalgo, P. Khabanov, A. Kozachek, L. Krupnik, M. Liniers, S. Lysenko, J. de Pablos, S. Sharapov, M. Ufimtsev, V. Zenin, and HIBP Group and TJ-II Team, *Nucl. Fusion* **56**, 112019 (2016).
- <sup>9</sup>Y. Hou, W. Chen, Y. Yu, M. Lesur, X. Duan, M. Xu, M. Y. Ye, and HL-2A Team, *Nucl. Fusion* **58**, 096028 (2018).
- <sup>10</sup>M. V. Zeeland, C. Collins, W. Heidbrink, M. Austin, X. Du, V. Duarte, A. Hyatt, G. Kramer, N. Gorelenkov, B. Grierson, D. Lin, A. Marinoni, G. McKee, C. Muscatello, C. Petty, C. Sung, K. Thome, M. Walker, and Y. Zhu, *Nucl. Fusion* **59**, 086028 (2019).
- <sup>11</sup>D. Maslovsky, B. Levitt, and M. E. Mael, *Phys. Rev. Lett.* **90**, 185001 (2003).
- <sup>12</sup>V. N. Duarte, N. N. Gorelenkov, M. Schneller, E. D. Fredrickson, M. Podestà, and H. L. Berk, *Nucl. Fusion* **58**, 082013 (2018).
- <sup>13</sup>S. D. Pinches, H. L. Berk, M. P. Gryaznevich, S. E. Sharapov, and JET-EFDA Contributors, *Plasma Phys. Controlled Fusion* **46**, S47 (2004).
- <sup>14</sup>H. L. Berk, B. N. Breizman, and N. V. Petviashvili, *Phys. Lett. A* **234**, 213 (1997).
- <sup>15</sup>H. L. Berk, B. N. Breizman, J. Candy, M. Pekker, and N. V. Petviashvili, *Phys. Plasmas* **6**, 3102 (1999).
- <sup>16</sup>H. S. Zhang, Z. Lin, and I. Holod, *Phys. Rev. Lett.* **109**, 025001 (2012).
- <sup>17</sup>A. Bierwage and K. Shinohara, *Phys. Plasmas* **23**, 042512 (2016).
- <sup>18</sup>V. N. Duarte, H. L. Berk, N. N. Gorelenkov, W. W. Heidbrink, G. J. Kramer, R. Nazikian, D. C. Pace, M. Podestà, B. J. Tobias, and M. A. Van Zeeland, *Nucl. Fusion* **57**, 054001 (2017).
- <sup>19</sup>G. Wang, H. Berk, B. Breizman, and L.-J. Zheng, *Nucl. Fusion* **58**, 082014 (2018).
- <sup>20</sup>B. J. Q. Woods, V. N. Duarte, A. J. De-Gol, N. N. Gorelenkov, and R. G. L. Vann, *Nucl. Fusion* **58**, 082015 (2018).
- <sup>21</sup>C. Slaby, A. Koenies, R. Kleiber, and H. Leyh, *Nucl. Fusion* **59**, 046006 (2019).
- <sup>22</sup>R. B. White, V. N. Duarte, N. N. Gorelenkov, E. D. Fredrickson, M. Podestà, and H. L. Berk, *Phys. Plasmas* **26**, 092103 (2019).
- <sup>23</sup>S. M. Kaye, M. Bell, R. Bell, S. Bernabei, J. Bialek, T. Biewer, W. Blanchard, J. Boedo, C. Bush *et al.*, *Nucl. Fusion* **45**, S168 (2005).
- <sup>24</sup>M. K. Lilley and R. M. Nyqvist, *Phys. Rev. Lett.* **112**, 155002 (2014).
- <sup>25</sup>R. B. White, *The Theory of Toroidally Confined Plasmas* (Imperial College Press, 2014).
- <sup>26</sup>N. N. Gorelenkov, C. Z. Cheng, and G. Fu, *Phys. Plasmas* **6**, 2802 (1999).
- <sup>27</sup>R. B. White and M. S. Chance, *Phys. Fluids* **27**, 2455 (1984).
- <sup>28</sup>Y. Chen, R. B. White, G.-Y. Fu, and R. Nazikian, *Phys. Plasmas* **6**, 226 (1999).

- <sup>29</sup>R. White, N. Gorelenkov, M. Gorelenkova, M. Podestà, S. Ethier, and Y. Chen, *Plasma Phys. Controlled Fusion* **58**, 115007 (2016).
- <sup>30</sup>C. Cheng, L. Chen, and M. Chance, *Ann. Phys.* **161**, 21 (1985).
- <sup>31</sup>E. Wigner, *Phys. Rev.* **40**, 749 (1932).
- <sup>32</sup>M. Bastiaans, *J. Opt. Soc. Am.* **69**, 1710 (1979).
- <sup>33</sup>R. F. Heeter, A. F. Fasoli, and S. E. Sharapov, *Phys. Rev. Lett.* **85**, 3177 (2000).
- <sup>34</sup>W. Chen, L. Yu, Y. Liu, X. Ding, H. Xie, J. Zhu, L. Yu, X. Ji, J. Li, Y. Li, D. Yu, Z. Shi, X. Song, J. Cao, S. Song, Y. Dong, W. Zhong, M. Jiang, Z. Cui, Y. Huang, Y. Zhou, J. Dong, M. Xu, F. Xia, L. Yan, Q. Yang, and X. Duan, and HL-2A Team, *Nucl. Fusion* **54**, 104002 (2014).
- <sup>35</sup>A. Bierwage, K. Shinohara, Y. Todo, N. Aiba, M. Ishikawa, G. Matsunaga, M. Takechi, and M. Yagi, *Nucl. Fusion* **57**, 016036 (2017).